ACS Medicinal Chemistry Letters

Cite This: ACS Med. Chem. Lett. 2019, 10, 1473−1479

Letter

pubs.acs.org/acsmedchemlett

Preclinical Development of PQR514, a Highly Potent PI3K Inhibitor Bearing a Difluoromethyl−Pyrimidine Moiety

Chiara Borsari,[†,§] Denise Rageot,[†,§] Florent Beaufils,[‡,§] Thomas Bohnacker,[†,§] Erhan Keles,[†] Ivan Buslov,[†] Anna Melone,[†] Alexander M. Sele,[†] Paul Hebeisen,[‡] Doriano Fabbro,[‡] Petra Hillmann,[‡] and Matthias P. Wymann*[,†]

[†]Department of Biomedicine, University of Basel, Mattenstrasse 28, 4058 Basel, Switzerland

[‡]PIQUR Therapeutics AG, Hochbergerstrasse 60, 4057 Basel, Switzerland

Supporting Information

ABSTRACT: The phosphoinositide 3-kinase (PI3K)/mechanistic target of rapamycin (mTOR) pathway is a critical regulator of cell growth and is frequently hyperactivated in cancer. Therefore, PI3K inhibitors represent a valuable asset in cancer therapy. Herein we have developed a novel anticancer agent, the potent pan-PI3K inhibitor PQR514 (**4**), which is a follow-up compound for the phase-II clinical compound PQR309 (**1**). Compound **4** has an improved potency both in vitro and in cellular assays with respect to its predecessor compounds. It shows superiority in the suppression of cancer cell proliferation and demonstrates significant antitumor activity in an OVCAR-3 xenograft model at concentrations approximately eight times lower than PQR309 (**1**). The favorable pharmacokinetic profile and a minimal brain penetration promote PQR514 (**4**) as an optimized candidate for the treatment of systemic tumors.

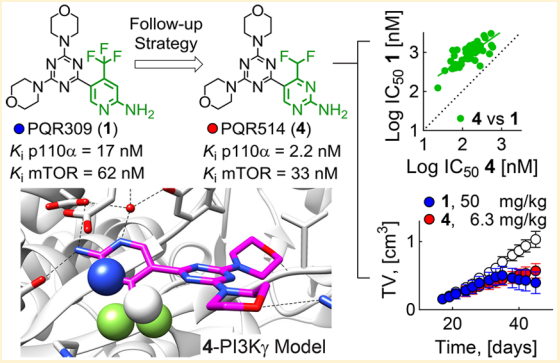

KEYWORDS: *Phosphoinositide 3-kinase (PI3K), mammalian or mechanistic target of rapamycin (mTOR); PI3K inhibitor, 4-(difluoromethyl)pyrimidin-2-amine, cancer; ATP-competitive; pharmacology, clinical candidate*

The phosphoinositide 3-kinase (PI3K)/mechanistic target of rapamycin (mTOR) signaling pathway plays a key role in many cellular processes, including cell growth, proliferation, and survival.[1,2] The PI3K family is divided into three classes according to their amino acid sequences, homology, and substrate specificity.[3] Class-I PI3Ks are activated downstream of cell surface receptors, including receptor protein tyrosine kinases (RTKs), G-protein-coupled receptors (GPCRs), and immunoglobulin receptors. Class-IA PI3Ks are obligate heterodimers composed of a catalytic subunit (p110α, p110β, or p110δ) and an associated regulatory subunit (p85α, p85β, p50α, p55α, or p55γ). The class-IB PI3Kγ operates downstream of GPCRs and consists of a catalytic subunit (p110γ) and an adapter subunit (p84 or p101).[4−6] Activated PI3K produces PtdIns(3,4,5)P_3, a docking site for protein kinase B (PKB/Akt) and 3-phosphoinositide-dependent protein kinase 1 (PDK1). Overactivation of this pathway can occur at multiple levels, finally promoting cancer growth and progression.[7] The loss or inactivation of the tumor suppressor phosphatase and tensin homologue (PTEN), the mutation or amplification of cell surface receptors, as well as the presence of activating hotspot mutations in PIK3CA play a key role in human carcinogenesis.[8] The PI3K/mTOR axis has been associated with resistance to multiple cancer treatments. Therefore, PI3K inhibitors are considered to be a valuable asset in cancer therapy. A considerable effort has been dedicated to the development of drugs targeting PI3K signaling, and many of them are currently being evaluated in clinical trials.[9] Besides monotherapy, PI3K inhibitors are tested as part of combination regimens.

Recently, we have reported on PQR309 (**1**, bimiralisib), a brain-penetrant pan-PI3K inhibitor, which also moderately targets mTOR kinase.[10−12] Compound **1** contains a 2-amino-4-(trifluoromethyl)pyridine linked to the triazine core (Figure 1A) and is currently in phase-II clinical trials for the treatment of lymphoma and solid tumors.[11] First phase-I clinical results have been disclosed.[13]

The effect of replacing the trifluoromethyl moiety with a difluoromethyl group has been investigated (compound **2**, Figure 1A), and the ability of the CHF_2 group to act as a lipophilic hydrogen donor in mTOR kinase has been pointed out to explain the improvement in mTOR affinity (K_i **1** = 62 nM; **2** = 6.9 nM, Table 1).[14] In addition, we have converted the pyridine ring of **1** into a pyrimidine moiety (**3**, Figure 1A). Compound **3** was a potent inhibitor of PI3K but not of mTOR (Table 1). Herein we have combined the two chemical

Received: July 22, 2019
Accepted: September 3, 2019
Published: September 3, 2019

DOI: 10.1021/acsmedchemlett.9b00333
ACS Med. Chem. Lett. 2019, 10, 1473−1479

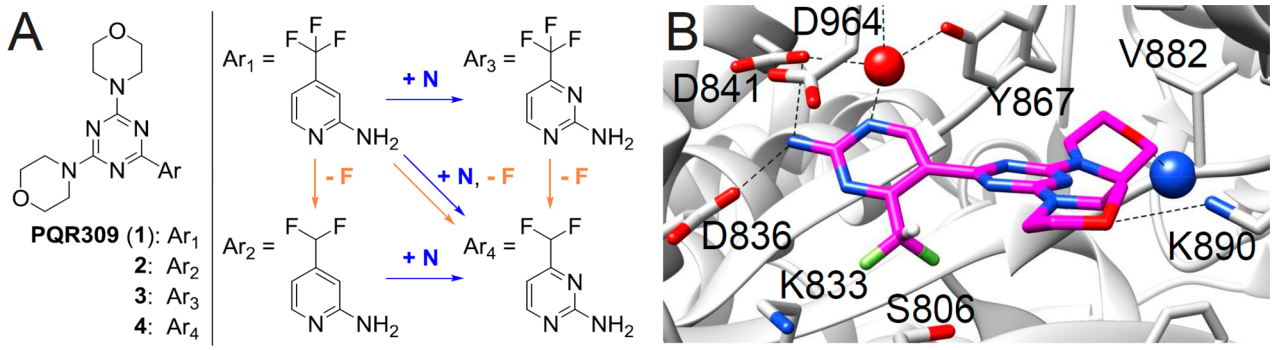

Figure 1. (A) Chemical modifications in the heteroaromatic moiety. Chemical structures of PQR309 (**1**),[11] **2**,[14] **3**,[11] and PQR514 (**4**). (B) Docking of PQR514 (**4**) (magenta) into PI3Kγ (gray) starting from PDB 5OQ4 (from ref 11). The structural water molecule is shown as a red ball. Water-mediated H bonds are depicted as dashed black lines. The Val882 backbone nitrogen involved in a H bond with the morpholine in the hinge region is shown as a blue ball.

Table 1. Cellular Potency and PI3K and mTOR Inhibitory Activity for Compounds 1−4

	cellular assays IC_{50} (nM)[a]		in vitro binding assays K_i (nM)[b]			
comp. name	pPKB S473	pS6 S235/236	p110α	mTOR	clogP[c]	PSA[c]
PQR309 (**1**)[d]	139	205	17	62	2.72	102.5
2[e]	102	118	12	6.9	2.07	102.5
3[d]	85	312	8.1	203	2.36	115.4
PQR514 (**4**)	17	61	2.2	33	1.58	115.4

[a]PKB phosphorylation on Ser473 and ribosomal S6 phosphorylation on Ser235/236 were analyzed in A2058 cells exposed to the indicated inhibitors and the subsequent detection of phosphoproteins in an in-cell Western assay. Each experiment performed with $n = 2$. [b]Compounds were tested for the in vitro binding to the ATP-binding site of p110α and mTOR using a commercially available time-resolved FRET (TR-FRET) displacement assay (LanthaScreen). Each experiment performed with $n = 2$. $lgIC_{50}$ values and standard errors are reported in Table S1. [c]Marvin/JChem 16.10.17 was used for the calculation of logP (partition coefficient) and PSA (polar surface area) values. [d]Data for compounds PQR309 (**1**) and **3** are shown for comparison and are from ref 11. [e]Data for compound **2** are from ref 14.

Scheme 1. Synthesis of Compounds 4−8[b]

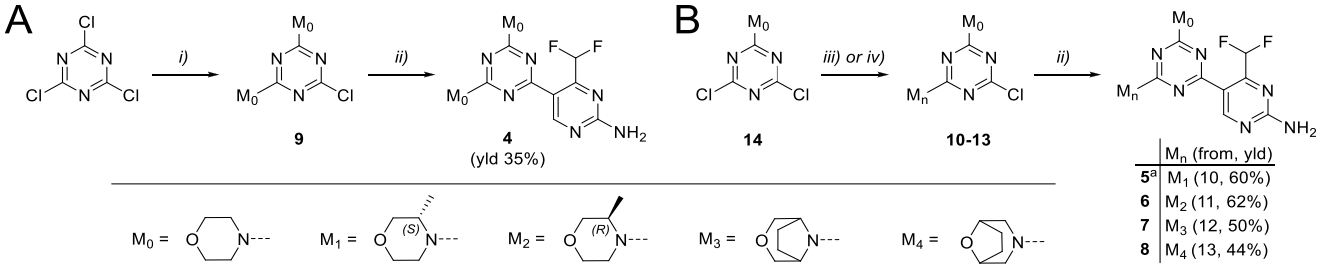

[a]Synthesis of compound **5** is reported in ref 16. [b]Reagents and conditions: (i) morpholine derivative (M_n−H), CH_2Cl_2, 0 °C → rt, o/n. (ii) (1) RBpin generated in situ (see the Supporting Information), $Pd(OAc)_2/PPh_3$ (cat.), K_2CO_3, THF, 60 °C, 2−4 h; (2) HCl, H_2O, 60 °C, 2 h. (iii) M_n−H, DIPEA, EtOH, 0 °C → rt, o/n. (iv) M_n−H, DIPEA, dioxane, 70 °C, o/n as reported in the literature.[16]

modifications of **2** and **3** to develop a novel, improved anticancer agent (Figure 1A). We propose the 4-(difluoromethyl)pyrimidin-2-amine as an optimized moiety for PI3K binding. Moreover, we report the preclinical characterization of PQR514 (**4**), a follow-up compound for **1**.

PQR514 (**4**) has been evaluated for in vitro binding (K_i for mTOR and PI3Kα (p110α)) and for PI3K/mTOR signaling in A2058 cells (IC_{50} for phosphorylated S6 ribosomal protein (pS6, Ser235/236) to detect mTORC1 activity and protein kinase B (PKB/Akt) phosphorylation on Ser473 to detect mTORC2 activity). Compound **4** was two times more potent on mTOR than the parental inhibitor **1**, whereas there was an almost eight-fold difference in PI3K inhibition (K_i(mTOR) **1** = 62 nM, **4** = 32.7 nM; K_i(p110α) **1** = 17 nM, **4** = 2.2 nM, Table 1). To explain the higher affinity for PI3K of the 4-(difluoromethyl)pyrimidin-2-amine compared with the CF_3-substituted pyridine, we analyzed interactions of compound **4** with the ATP-binding site. The X-ray crystal structure of PQR309 (**1**) in PI3Kγ had been solved at a 2.7 Å resolution, and the key interactions have been identified (see ref 11; PDB code 5OQ4). We have substituted **1** with **4** and performed energy minimization. The resulting PI3Kγ-**4** complex showed major interactions such as H bonds between the amino-pyrimidine and Asp836/964, and between a morpholine oxygen atom and the backbone amide of Val882. The other solvent-exposed morpholine is stabilized by a H bond between its oxygen atom and the side chain of Lys890 (distance = 3.2 Å, Figure 1B). The CHF_2-group could interact with (i) Asp836 or (ii) a triazine core nitrogen, as previously suggested.[14] The presence of many hydrophilic amino acids in the binding pocket of the heteroaromatic ring suggested that a pyrimidine might be better accommodated than a pyridine. The nitrogen

DOI: 10.1021/acsmedchemlett.9b00333
ACS Med. Chem. Lett. 2019, 10, 1473−1479

Table 2. Proof-of-Concept Compounds Bearing a 4-(Difluoromethyl)pyrimidin-2-amine Moiety

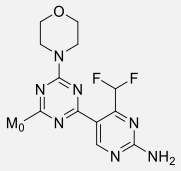

Name	M_n	Cellular Assays IC_{50} [nM][a] pPKB S473	pS6 S235/236	in vitro Binding Assays K_i [nM][b] p110α	mTOR	clogP[c]
PQR514 (4)	M_0	17	61	2.2	33	1.58
5[d]	M_1	32	64	1.9	11	1.99
6	M_2	64	116	2.7	21	1.99
7	M_3	73	91	3.4	14	2.08
8	M_4	84	139	4.4	29	2.08

[a]PKB phosphorylation on Ser473 and ribosomal S6 phosphorylation on Ser235/236 were analyzed in A2058 cells exposed to the indicated inhibitors and the subsequent detection of phosphoproteins in an in-cell Western assay. Each experiment performed with $n = 2$. Chemical structures of M_0–M_4 are depicted in Scheme 1 [b]Compounds were tested for the in vitro binding to the ATP-binding site of p110α and mTOR using a commercially available time-resolved FRET (TR-FRET) displacement assay (LanthaScreen). Each experiment performed with $n = 2$. $lgIC_{50}$ values and standard errors are reported in Table S1. [c]Marvin/JChem 16.10.17 was used for the calculation of logP (partition coefficient) and PSA (polar surface area) values. [d]Data for compound **5** are from ref 16.

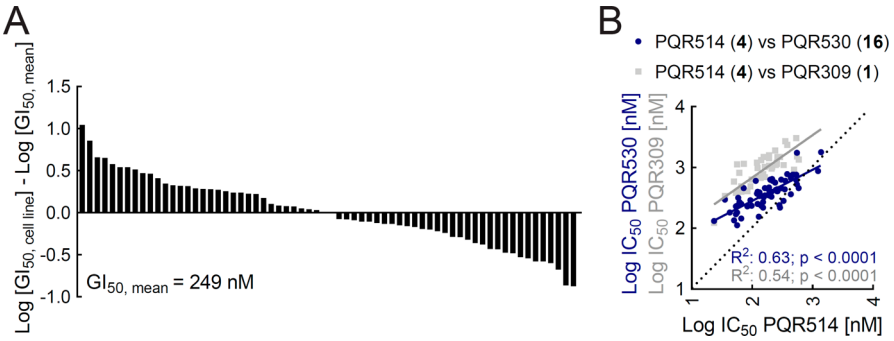

Figure 2. (A) Waterfall plot of compound PQR514 (**4**) in a full NTRC (Netherlands Translational Research Center BV) Oncolines cell panel of 66 cancer cell lines. Concentrations of half-maximal growth inhibition (GI_{50}) for **4** were obtained from dose–response growth curves, and individual GC_{50} values of a cell line were related to the mean GI_{50} of all cell lines; cell lines were sorted by lowest to highest sensitivity for **4**. Individual cell line names and GI_{50} values are reported in Table S7. (B) Cellular inhibition profile of PQR514 (**4**), PQR309 (**1**), and PQR530 (**16**). The correlation of log-(IC_{50}) in nanomoles for the inhibition of cell proliferation in 44 tumor cell lines is depicted. R^2 and p values are from the nonparametric Spearman's correlation. Dashed line: perfect correlation with identical IC_{50} values. Blue line: linear regression for PQR514 (**4**) versus PQR530 (**16**). Gray line: linear regression for PQR514 (**4**) versus PQR309 (**1**). $LogIC_{50}$ data of PQR309 (**1**) and PQR530 (**16**) were extracted from ref 16.

Table 3. Stability of Compound PQR514 (4) in Liver Microsomes

% remaining compound after 30 min[a]			
rat	mouse	dog	human
109 ± 10.7	82.4 ± 10.9	92.7 ± 0.2	87.2 ± 3.5

[a]Experiments were carried out by Aphad S.r.l. with rat, mouse, dog and human liver microsomes (Xenotech). Each experiment performed with $n = 2$. Assay reference compounds: 7-ethoxycoumarin and propranolol.

Table 5. PK Analysis of PQR514 (4) after Oral Application in Male C57BL/6J Mice (10 mg/kg p.o.)[a]

	plasma	brain	thigh muscle
C_{max} (ng/mL)	3282	1023	1808
T_{max} (h)	1.0	0.5	0.5
$t_{1/2}$ (h)	1.7	1.6	1.6
$AUC_{0\text{-}8h}$ (h*ng/mL)	10315	2757	4526
Cl (mL/h/kg)	934	3519	2147

[a]p.o.: per os; C_{max}: maximal concentration, T_{max}: time of maximal concentration in hours; $t_{1/2}$: half-life elimination in hours; AUC: area under the curve, Cl: clearance ($n = 3$, mean for each time point).

Table 4. Stability of Compound PQR514 (4) in Hepatocytes

clearance (μL/min/10^6 cells)[a]				stability $t_{1/2}$ (min)[a]			
rat	mouse	dog	human	rat	mouse	dog	human
1.5 ± 0.7[b]	7.0 ± 1.4	6.7 ± 1.2	4.0 ± 0.1	520 ± 245[b]	192.5 ± 33.3	211.7 ± 33.3	346.5 ± 0.1

[a]Experiments were carried out by Aphad S.r.l. with rat, mouse, dog and human hepatocytes. Each experiment performed with $n = 3$. [b]Variability due to very low clearance.

DOI: 10.1021/acsmedchemlett.9b00333
ACS Med. Chem. Lett. 2019, 10, 1473–1479

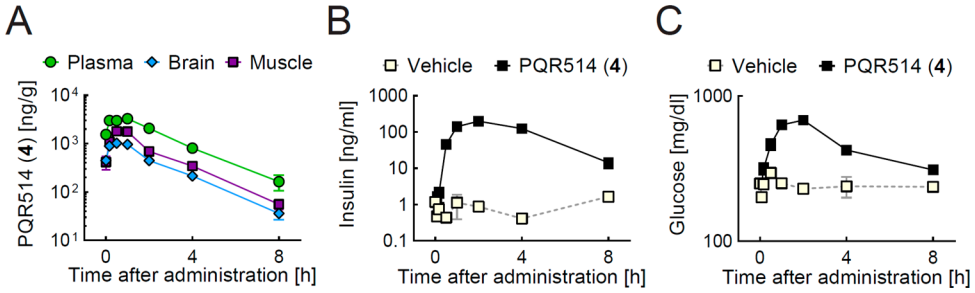

Figure 3. PK/PD assessment of PQR514 (**4**). Compound **4** was administered to male C57BL/6J mice as a single dose per os (p.o., 10 mg/kg). (A) Levels of **4** in male C57BL/6J mice tissues: plasma, brain, and thigh muscle (n = 3). Compound **4** was extracted from each tissue at the indicated time points and quantified using LC−MS. (B) Glucose and (C) insulin plasma levels after the oral administration of **4** in male C57BL/6J mice. All values: mean ± SEM. Error bars not shown are smaller than the symbols. Values are reported in Tables S11 and S12.

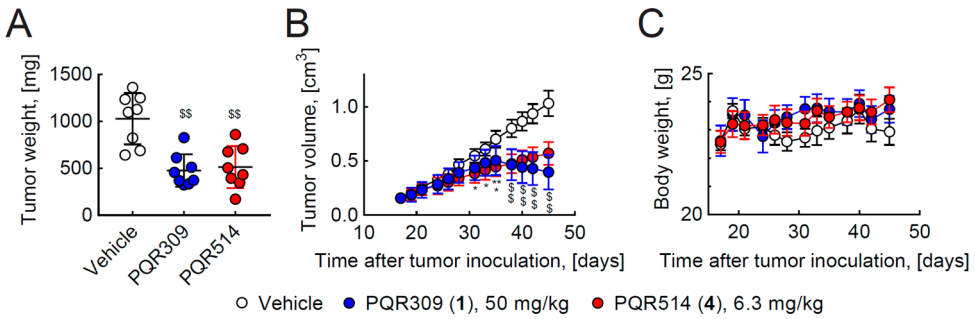

Figure 4. OVCAR-3 human ovarian cancer xenograft model in BALB/c nude mice: Tumor cells were subcutaneously inoculated at day 0, and the daily oral application of the indicated agents was started at day 17 (28 × QD). (A) Tumor weight was determined at day 45. (B) Tumor size was measured and calculated as described in the text. (C) Body weight was determined at the depicted time points. Statistics: $^{*}p < 0.05$, $^{**}p < 0.001$, $^{\$}p < 0.0001$, n = 8. (A) One-way ANOVA with Tukey's correction for multicomparisons, mean ± SEM. PQR309 (**1**) and vehicle data were reprinted from ref 11. (B,C) Two-way ANOVA with Bonferroni or Dunnett's correction for multicomparisons, mean ± SEM. (B) Statistic symbols: above, PQR309 (**1**); below, PQR514 (**4**).

in position three of the pyrimidine core is in proximity to Lys833 (<5 Å), and thus a H bond might stabilize the inhibitor binding to PI3Kγ. Given the high homology of the ATP-binding pocket of class-I PI3Ks and mTOR, an identical binding mode for all PI3K isoforms and mTOR can be assumed. The above-described interactions could explain the higher in vitro potency of compound **4** compared with PQR309 (**1**). To confirm the superiority of the 4-(difluoromethyl)pyrimidin-2-amine for inhibitor binding, four proof-of-concept compounds (**5**−**8**) were synthesized. One morpholine of inhibitor **4** was replaced with different substituted morpholines (M_n), such as 3-methylmorpholine (M_1: (S) and M_2: (R)), 3-oxa-8-azabicyclo[3.2.1]octane (M_3), and 8-oxa-3-azabicyclo[3.2.1]octane (M_4). The procedures followed for the synthesis of compounds **4**−**8** are depicted in Scheme 1. For the synthesis of compound **4**, 4,4′-(6-chloro-1,3,5-triazine-2,4-diyl)dimorpholine (**9**) was prepared starting from the commercially available 2,4,6-trichlorotriazine. The chlorine of intermediate **9** was displaced by 4-(difluoromethyl)pyrimidin-2-amine using a Suzuki cross-coupling reaction with the boronic acid pinacol ester generated in situ (see Scheme 1A and the Supporting Information for details). For asymmetric compounds **5**−**8**, the substituted morpholine (M_n) was introduced starting from 2,4-dichloro-6-(morpholin-4-yl)-1,3,5-triazine (**14**), and subsequent palladium-catalyzed Suzuki coupling gave the final compounds in moderate to good yield (44−62%).

All of the synthesized compounds were highly potent PI3K inhibitors (K_i(p110α) < 4.5 nM), also showing a good affinity for mTOR kinase (K_i(mTOR) < 35 nM). These results confirmed the 4-(difluoromethyl)pyrimidin-2-amine as an optimized binding module compared with the CF_3−pyridine of compound **1**. Compounds **4**−**8** were more potent both in vitro and in cells than compound **1** (Tables 1 and 2). Among the CHF_2−pyrimidine derivatives, PQR514 (**4**) had a superior activity in cells (IC_{50} for phosphorylated PKB/Akt = 17 nM, IC_{50} for phosphorylated S6 = 61 nM) and was chosen for further characterization using the KINOMEScan platform of DiscoverX. DiscoverX KdELECT assays confirmed the excellent affinity for PI3Ks of **4** (K_d PI3K$\alpha/\beta/\delta/\gamma$ < 7 nM, Table S2). Moreover, PQR514 (**4**) was screened in a KINOMEScan panel for interactions with a wide range of proteins (>400) and lipid kinases to validate its specificity. At a 10 μM concentration, it showed negligible interference with protein kinase activities (Figure S1 and Table S3) and reached excellent selectivity scores of $S(35)$ = 0.041 and $S(10)$ = 0.025, calculated according to ref 15 (Table S4). To evaluate off-target effects, compound **4** was tested in a CEREP BioPrint (P22-p) panel at a concentration of 10 μM. With the exception of human PDE3A (phosphodiesterase 3A), no or very weak interactions were detected (Tables S5 and S6). These data qualify PQR514 (**4**) as a selective pan-PI3K inhibitor.

In addition, **4** was screened using a fluorescence high-throughput P450 assay to exclude the inhibition of cytochrome P450 (CYP) enzymes. PQR514 (**4**) showed half-maximal inhibitory concentration (IC_{50}) >100 μM for all of the P450 isoenzymes tested (CYP1A2, CYP2C19, CYP2D6, and CYP3A4), highlighting the safety profile of the molecule.

PQR514 (**4**) was tested in vitro across a panel of 66 tumor cells: Compound **4** showed potency across these cell lines with

DOI: 10.1021/acsmedchemlett.9b00333
ACS Med. Chem. Lett. 2019, 10, 1473−1479

a mean half-maximal growth inhibition (GI_{50}) of 0.25 μM (Figure 2A). A comparison with the structurally related PQR309[11] (**1**, GI_{50} ~1 μM) and PQR530 (**16**, GI_{50} ~0.4 μM; see Figure S2 and ref 16 for the chemical structure) pointed out the superiority of PQR514 (**4**) (GI_{50} of 0.24 μM) in the suppression of cancer cell proliferation in a matched 44 cell line panel (Figure 2B and Table S7).

A PAMPA (parallel artificial membrane permeability assay) was performed, and PQR514 (**4**) showed a high passive permeability (81.96 ± 5.40 nm/s). As an additional indicator of bioavailability, the thermodynamic solubility over a range of pH values as well as in fasted and fed state simulated intestinal fluids (FaSSIF and FeSSIF) was measured (Table S8). A correlation between solubility, estimated intestinal permeability, and projected clinical potency has been outlined, and even for most potent and highly permeable compounds, a thermodynamic solubility of at least 1 μg/mL is favorable. Compound **4** displayed a solubility >1 μg/mL at all pH values tested, with a maximum at pH 1.2 (13.6 μg/mL, Table S8), and thus matched criteria for drug-like compounds.

To assess the in vitro metabolic stability of **4**, it was exposed to microsomes and hepatocytes of different origins. PQR514 (**4**) was only minimally metabolized when incubated with rat, mouse, dog and human liver microsomes, as indicated by, respectively, 109, 82.4, 92.7, and 87.2% remaining compound after 30 min of exposure (Table 3). The high stability of **4** in microsomal assays was consistent with clearance and half-life measurements in rat, mouse, dog, and human hepatocyte cultures. PQR514 (**4**) showed a low clearance in all species. The half life of **4** was 5.8 h in human hepatocytes and 3.2−8.7 h in the other species (Table 4).

PQR514 (**4**) was then profiled in vivo in mice to evaluate the pharmacological parameters and determine the optimal dosing schedule for efficacy studies. A single oral dose of 10 mg/kg was administered to male C57BL/6J mice, and concentrations of **4** in plasma, brain, and thigh muscle were monitored over time. Pharmacokinetic (PK) parameters are summarized in Table 5. The maximal concentration (C_{max}) of PQR514 (**4**) was reached in plasma after 1 h (3282 ng/mL) and in brain and thigh muscle after 30 min (1023 and 1808 ng/g, respectively) (Figure 3A and Table 5). Compound **4** showed limited brain access and showed a ca. 1:0.3 distribution between plasma and brain. The minimal brain permeability of **4** suggests the possible application in the treatment of systemic tumors,[17] avoiding putative neurological side effects. Neuropsychiatric effects such as anxiety and depression had been observed in patients treated with brain penetrant BKM120 (buparlisib), a pan PI3K inhibitor with microtubule-destabilizing activity,[10] but did not become apparent in a PQR309 (**1**) phase-I study.[13]

The administration of compound **4** in male C57BL/6J mice triggered a rapid increase in plasma insulin and glucose levels. The plasma insulin and glucose levels reached a maximal concentration 2 h after dosing (Figure 3B,C, respectively). This rise is a reliable marker for the on-target action of PQR514 (**4**) and has been observed with other PI3K inhibitors, including PQR309 (**1**).[11,18]

To assess the in vivo antiproliferative effect of compound **4**, an OVCAR-3 xenograft model in BALB/c nude mice was used: Each mouse was inoculated subcutaneously with 5×10^6 OVCAR-3 tumor cells for tumor development. From day 17 on, the control group received the vehicle once a day (QD), whereas the treated groups received either 6.3 mg/kg of compound **4** p.o. or 50 mg/kg of compound **1** p.o. QD for 28 days. The mean tumor size of the vehicle-treated group reached 1031 mm^3 on day 45 after tumor inoculation. Treatment with **4** led to a significant antitumor activity: The mean tumor size was 397 mm^3, as compared with 571 mm^3 after treatment with PQR309 (**1**) at an eight times higher dose than **4** (6.3 vs 50 mg/kg, Figure 4A). The results of the tumor weight analysis were consistent with the tumor volume analysis: Compared with vehicle-treated mice, compound **4** significantly inhibited tumor growth (Figure 4B). PQR514 (**4**) was well tolerated at 6.3 mg/kg, and no significant body weight loss was observed (Figure 4C). In vivo toxicokinetic studies were carried out to assess the toxic potential of compound **4** and to establish the maximum tolerated dose (MTD). A 14-day pilot study with PQR514 (**4**) was carried out in Wistar rats and beagle dogs, and the toxicokinetic parameters are summarized in Table S9. In Wistar rats, the no-observed adverse effect level (NOAEL) of compound **4** was considered to be 2.4 mg/kg/day for females and 3.6 mg/kg/day for males. In beagle dogs, the NOAEL of compound **4** was 10 mg/kg/day.

In summary, we have characterized the 4-(difluoromethyl)-pyrimidin-2-amine moiety as an optimized residue for PI3K binding and proposed PQR514 (**4**) as a novel anticancer agent that can serve as a follow-up compound for PQR309 (**1**).[10,11,13] Compound **4** demonstrated significant antitumor activity in a mice xenograft model at a concentration almost eight times lower than the parental phase-II inhibitor (**1**). On the basis of its remarkable PI3K affinity, favorable pharmacological parameters, safety profile, and in vivo antitumor efficacy, PQR514 (**4**) qualifies as a targeted anticancer drug with a potential application in the treatment of systemic tumors.

■ ASSOCIATED CONTENT

Supporting Information

The Supporting Information is available free of charge on the ACS Publications website at DOI: 10.1021/acsmedchemlett.9b00333.

Synthesis and characterization of compounds. Experimental section. Compiled activity data and standard errors (SEM) (Table S1). Lipid kinases and mTOR binding constants of PQR514 (**4**) and PQR309 (**1**) (Table S2). TREEspot data visualization of KINOMEscan interactions of PQR514 (**4**) and PQR309 (**1**) at 10 μM (Figure S1). Kinase interactions of PQR514 (**4**) and PQR309 (**1**) at 10 μM (KINOMEscan) (Table S3). Selectivity profile of PQR514 (**4**) calculated from KINOMEscan data (Table S4). In vitro pharmacology I − ligand binding assays with PQR514 (**4**) at 10 μM (Table S5). In vitro pharmacology II − enzyme assays with PQR514 (**4**) at 10 μM (Table S6). Impact of PQR514 (**4**), PQR309 (**1**), and PQR530 (**16**) on cell proliferation (Table S7). Physicochemical properties of PQR514 (**4**) (Table S8). Safety profile of PQR514 (**4**) (Table S9). ^{1}H NMR spectra of final compounds. ^{13}C NMR spectra of final compounds. HRMS spectra of final compounds. HPLC chromatograms of final compounds. Chemical structures (Figure S2) (PDF)

DOI: 10.1021/acsmedchemlett.9b00333
ACS Med. Chem. Lett. 2019, 10, 1473−1479

AUTHOR INFORMATION

Corresponding Author

*Tel: +41 61 207 5046. Fax: +41 61 207 3566. E-mail: Matthias.Wymann@UniBas.CH.

ORCID

Chiara Borsari: 0000-0002-4688-8362
Denise Rageot: 0000-0002-2833-5481
Alexander M. Sele: 0000-0002-4903-7934
Matthias P. Wymann: 0000-0003-3349-4281

Author Contributions

§C.B., D.R., F.B., and T.B. contributed equally to this work. The manuscript was written through contributions of all authors. All authors have given approval to the final version of the manuscript.

Funding

This work was supported by the Swiss Commission for Technology and Innovation (CTI) by PFLS-LS grants 14032.1, 15811.2, and 17241.1, the Stiftung für Krebsbekämpfung grant 341, and Swiss National Science Foundation grants 310030_153211 and 316030_133860 (to M.P.W.).

Notes

The authors declare the following competing financial interest(s): F.B., P.He., P.Hi., and D.F. are current or past employees of PIQUR Therapeutics AG, Basel, and P.He., D.F., and M.P.W. are shareholders of PIQUR Therapeutics AG.

ACKNOWLEDGMENTS

We thank A. Pfaltz, R. A. Ettlin, W. Dieterle, S. Mukherjee, J. Mestan, and M. Lang for advice and discussions; S. Bünger and A. Dall'Asen for technical assistance; and M. Pfeffer and the mass spectrometry and elemental analysis team at the University of Basel for HRMS data.

ABBREVIATIONS

PI3K, phosphoinositide 3-kinase; RTKs, receptor tyrosine kinases; GPCRs, G-protein-coupled receptors; PTEN, phosphatase and tensin homologue; PKB/Akt, protein kinase B; PDK1, phosphoinositide-dependent protein kinase 1; S6K, p70 S6 kinase; VPS34, vacuolar protein sorting 34 (the class-III PI3K); mTOR, mechanistic (or mammalian) target of rapamycin; TORC1, mTOR complex 1; TORC2, mTOR complex 2; DIPEA, *N*,*N*-diisopropylethylamine; PK, pharmacokinetic; TR-FRET, time-resolved Förster resonance energy transfer

REFERENCES

(1) Wymann, M. P.; Schneiter, R. Lipid signalling in disease. *Nat. Rev. Mol. Cell Biol.* **2008**, *9* (2), 162−176.

(2) Marone, R.; Cmiljanovic, V.; Giese, B.; Wymann, M. P. Targeting phosphoinositide 3-kinase: moving towards therapy. *Biochim. Biophys. Acta, Proteins Proteomics* **2008**, *1784* (1), 159−185.

(3) Fruman, D. A.; Rommel, C. PI3K and cancer: lessons, challenges and opportunities. *Nat. Rev. Drug Discovery* **2014**, *13* (2), 140−56.

(4) Bohnacker, T.; Marone, R.; Collmann, E.; Calvez, R.; Hirsch, E.; Wymann, M. P. PI3Kγ Adaptor Subunits Define Coupling to Degranulation and Cell Motility by Distinct PtdIns(3,4,5)P_3 Pools in Mast Cells. *Sci. Signaling* **2009**, *2* (74), ra27−ra27.

(5) Hirsch, E.; Katanaev, V. L.; Garlanda, C.; Azzolino, O.; Pirola, L.; Silengo, L.; Sozzani, S.; Mantovani, A.; Altruda, F.; Wymann, M. P. Central Role for G Protein-Coupled Phosphoinositide 3-Kinase γ in Inflammation. *Science* **2000**, *287* (5455), 1049−1053.

(6) Wymann, M. P.; Sozzani, S.; Altruda, F.; Mantovani, A.; Hirsch, E. Lipids on the move: phosphoinositide 3-kinases in leukocyte function. *Immunology Today* **2000**, *21* (6), 260−264.

(7) Fruman, D. A.; Chiu, H.; Hopkins, B. D.; Bagrodia, S.; Cantley, L. C.; Abraham, R. T. The PI3K Pathway in Human Disease. *Cell* **2017**, *170* (4), 605−635.

(8) Arteaga, C. L.; Sliwkowski, M. X.; Osborne, C. K.; Perez, E. A.; Puglisi, F.; Gianni, L. Treatment of HER2-positive breast cancer: current status and future perspectives. *Nat. Rev. Clin. Oncol.* **2012**, *9* (1), 16−32.

(9) Yang, J.; Nie, J.; Ma, X.; Wei, Y.; Peng, Y.; Wei, X. Targeting PI3K in cancer: mechanisms and advances in clinical trials. *Mol. Cancer* **2019**, *18* (1), 26.

(10) Bohnacker, T.; Prota, A. E.; Beaufils, F.; Burke, J. E.; Melone, A.; Inglis, A. J.; Rageot, D.; Sele, A. M.; Cmiljanovic, V.; Cmiljanovic, N.; Bargsten, K.; Aher, A.; Akhmanova, A.; Diaz, J. F.; Fabbro, D.; Zvelebil, M.; Williams, R. L.; Steinmetz, M. O.; Wymann, M. P. Deconvolution of Buparlisib's mechanism of action defines specific PI3K and tubulin inhibitors for therapeutic intervention. *Nat. Commun.* **2017**, *8*, 14683.

(11) Beaufils, F.; Cmiljanovic, N.; Cmiljanovic, V.; Bohnacker, T.; Melone, A.; Marone, R.; Jackson, E.; Zhang, X.; Sele, A.; Borsari, C.; Mestan, J.; Hebeisen, P.; Hillmann, P.; Giese, B.; Zvelebil, M.; Fabbro, D.; Williams, R. L.; Rageot, D.; Wymann, M. P. 5-(4,6-Dimorpholino-1,3,5-triazin-2-yl)-4-(trifluoromethyl)pyridin-2-amine (PQR309), a Potent, Brain-Penetrant, Orally Bioavailable, Pan-Class I PI3K/mTOR Inhibitor as Clinical Candidate in Oncology. *J. Med. Chem.* **2017**, *60* (17), 7524−7538.

(12) Tarantelli, C.; Gaudio, E.; Arribas, A. J.; Kwee, I.; Hillmann, P.; Rinaldi, A.; Cascione, L.; Spriano, F.; Bernasconi, E.; Guidetti, F.; Carrassa, L.; Pittau, R. B.; Beaufils, F.; Ritschard, R.; Rageot, D.; Sele, A.; Dossena, B.; Rossi, F. M.; Zucchetto, A.; Taborelli, M.; Gattei, V.; Rossi, D.; Stathis, A.; Stussi, G.; Broggini, M.; Wymann, M. P.; Wicki, A.; Zucca, E.; Cmiljanovic, V.; Fabbro, D.; Bertoni, F. PQR309 Is a Novel Dual PI3K/mTOR Inhibitor with Preclinical Antitumor Activity in Lymphomas as a Single Agent and in Combination Therapy. *Clin. Cancer Res.* **2018**, *24* (1), 120−129.

(13) Wicki, A.; Brown, N.; Xyrafas, A.; Bize, V.; Hawle, H.; Berardi, S.; Cmiljanovic, N.; Cmiljanovic, V.; Stumm, M.; Dimitrijevic, S.; Herrmann, R.; Pretre, V.; Ritschard, R.; Tzankov, A.; Hess, V.; Childs, A.; Hierro, C.; Rodon, J.; Hess, D.; Joerger, M.; von Moos, R.; Sessa, C.; Kristeleit, R. First-in human, phase 1, dose-escalation pharmacokinetic and pharmacodynamic study of the oral dual PI3K and mTORC1/2 inhibitor PQR309 in patients with advanced solid tumors (SAKK 67/13). *Eur. J. Cancer* **2018**, *96*, 6−16.

(14) Rageot, D.; Bohnacker, T.; Melone, A.; Langlois, J. B.; Borsari, C.; Hillmann, P.; Sele, A. M.; Beaufils, F.; Zvelebil, M.; Hebeisen, P.; Loscher, W.; Burke, J.; Fabbro, D.; Wymann, M. P. Discovery and Preclinical Characterization of 5-[4,6-Bis({3-oxa-8-azabicyclo[3.2.1]-octan-8-yl})-1,3,5-triazin-2-yl]-4-(difluoro methyl)pyridin-2-amine (PQR620), a Highly Potent and Selective mTORC1/2 Inhibitor for Cancer and Neurological Disorders. *J. Med. Chem.* **2018**, *61* (22), 10084−10105.

(15) Karaman, M. W.; Herrgard, S.; Treiber, D. K.; Gallant, P.; Atteridge, C. E.; Campbell, B. T.; Chan, K. W.; Ciceri, P.; Davis, M. I.; Edeen, P. T.; Faraoni, R.; Floyd, M.; Hunt, J. P.; Lockhart, D. J.; Milanov, Z. V.; Morrison, M. J.; Pallares, G.; Patel, H. K.; Pritchard, S.; Wodicka, L. M.; Zarrinkar, P. P. A quantitative analysis of kinase inhibitor selectivity. *Nat. Biotechnol.* **2008**, *26* (1), 127−132.

(16) Rageot, D.; Bohnacker, T.; Keles, E.; McPhail, J. A.; Hoffmann, R. M.; Melone, A.; Borsari, C.; Sriramaratnam, R.; Sele, A. M.; Beaufils, F.; Hebeisen, P.; Fabbro, D.; Hillmann, P.; Burke, J. E.; Wymann, M. P. (S)-4-(Difluoromethyl)-5-(4-(3-methylmorpholino)-6-morpholino-1,3,5-triazin-2-yl)p yridin-2-amine (PQR530), a Potent, Orally Bioavailable, and Brain-Penetrable Dual Inhibitor of Class I PI3K and mTOR Kinase. *J. Med. Chem.* **2019**, *62* (13), 6241−6261.

(17) Borsari, C.; Rageot, D.; Dall'Asen, A.; Bohnacker, T.; Melone, A.; Sele, A. M.; Jackson, E.; Langlois, J. B.; Fabbro, D.; Hillmann, P.; Hebeisen, P.; Wymann, M. P. A conformational restriction strategy

DOI: 10.1021/acsmedchemlett.9b00333
ACS Med. Chem. Lett. 2019, 10, 1473−1479

for the identification of a highly selective pyrimido-pyrrolo-oxazine mTOR inhibitor. *J. Med. Chem.* [Online early access] DOI: 10.1021/acs.jmedchem.9b00972. Published online August 29, **2019**. https://pubs.acs.org/doi/10.1021/acs.jmedchem.9b00972.

(18) Hopkins, B. D.; Pauli, C.; Du, X.; Wang, D. G.; Li, X.; Wu, D.; Amadiume, S. C.; Goncalves, M. D.; Hodakoski, C.; Lundquist, M. R.; Bareja, R.; Ma, Y.; Harris, E. M.; Sboner, A.; Beltran, H.; Rubin, M. A.; Mukherjee, S.; Cantley, L. C. Suppression of insulin feedback enhances the efficacy of PI3K inhibitors. *Nature* **2018**, *560* (7719), 499−503.

DOI: 10.1021/acsmedchemlett.9b00333
ACS Med. Chem. Lett. 2019, 10, 1473−1479